



Cite this: *Soft Matter*, 2016, 12, 6799

A polymer microgel at a liquid–liquid interface: theory vs. computer simulations

Artem M. Romyantsev,^{ab} Rustam A. Gumerov^a and Igor I. Potemkin^{*ab}

We propose a mean-field theory and dissipative particle dynamics (DPD) simulations of swelling and collapse of a polymer microgel adsorbed at the interface of two immiscible liquids (A and B). The microgel reveals surface activity and lowers A–B interfacial tension. Attempting to occupy as large an interfacial area as possible, the microgel undergoes anisotropic deformation and adopts a flattened shape. Spreading over the interface is restricted by polymer subchain elasticity. The equilibrium shape of the microgel at the interface depends on its size. Small microgels are shown to be more oblate than the larger microgels. Increasing microgel cross-link density results in stronger reduction of the surface tension and weaker flattening. As the degree of immiscibility of A and B liquids increases, the microgel volume changes in a non-monotonous fashion: the microgel contraction at moderate immiscibility of A and B liquids is followed by its swelling at high incompatibility of the liquids. The segregation regime of the liquids within and outside the microgel is different. Being segregated outside the microgel, the liquids can be fully (homogeneously) mixed or weakly segregated within it. The density profiles of the liquids and the polymer were plotted under different conditions. The theoretical and the DPD simulation results are in good agreement. We hope that our findings will be useful for the design of stimuli responsive emulsions, which are stabilized by the microgel particles, as well as for their practical applications, for instance, in biocatalysis.

Received 28th May 2016,
Accepted 18th July 2016

DOI: 10.1039/c6sm01231k

www.rsc.org/softmatter

1 Introduction

It has been recently found that polymer microgel particles possess high surface activity and efficiently stabilize emulsions.^{1–5} The microgels adsorb at a liquid–liquid interface and reduce the interfacial tension like solid colloidal particles in Pickering emulsions.^{6,7} Due to the softness and deformability of the cross-linked polymer particles, microgel-stabilized emulsions find a wide range of practical applications. For instance, high sensitivity of the microgels to the external stimuli such as temperature, low-molecular-weight salts and pH allows controlling the stability of the emulsions and breaks them on demand.^{4,5,8–10}

A very promising behavior of the microgel-stabilized emulsions in comparison with the Pickering emulsions is caused by the differences in the physical properties of the polymer microgels and the solid colloidal particles. First, the microgels are soft and deformable. Being adsorbed at the liquid–liquid interface, the microgels spread over it and adopt a ‘fried-egg’ shape, while they are spherical in each of the liquids.^{11,12} Flattening of the microgels, induced by their ability to diminish the interfacial tension, is restricted by the elasticity of the microgel subchains. Second, the adsorbed microgels are penetrable for the molecules of both liquids.

Therefore, the parts of the microgels exposed to the different liquids are able to swell or collapse differently depending on the solvent quality of the liquids. The amount of absorbed liquids and preferential immersion of the microgels also depend on the solubility of the polymer in the liquids. For instance, the poly(*N*-isopropylacrylamide-*co*-methacrylic acid) [NiPAM-*co*-MAA] microgel is soluble in water and polar oil 1-octanol, while insoluble in nonpolar oil *n*-heptane.^{12–14} Emulsions of both these oils in water can be stabilized by this microgel, however the degree of immersion of the adsorbed microgels and the curvature of the interface (the droplet size) are different for these systems.^{12–14} The presence of microgels at the interfaces of polar and nonpolar oils diminishes the number of unfavorable contacts between immiscible molecules of water and oil by substituting them on polymer–water and polymer–oil contacts. This mechanism underlies the reduction of interfacial tension by the microgels and explains their surface activity.

Microgel permeability as well as sensitivity to the external stimuli makes the microgel-stabilized emulsions attractive for biocatalysis applications. If substrates and products are poorly soluble in water, reactions should be carried out in the emulsion since enzymes being proteins possess better solubility and catalytic activity in the aqueous media. Stabilization of the emulsion by thermosensitive microgels adsorbed at the interface of oil droplets was undertaken in ref. 15. Substrate and product molecules readily penetrated through the microgels

^a Physics Department, Lomonosov Moscow State University, 119991 Moscow, Russian Federation. E-mail: igor@poly.phys.msu.ru

^b DWI – Leibniz Institute for Interactive Materials, Aachen 52056, Germany

which provided emulsion stability at the temperature below VPTT. As soon as the enzyme-catalyzed reaction was finished, the emulsion was broken by moderate heating so that the product could be easily extracted from the oil phase. After the addition of a new substrate and repeated emulsion preparation, this process could be carried out again. Thus, the use of sensitive microgels allows us not only to speed up the reaction due to the high penetrability of the microgels but also to avoid enzyme denaturation thanks to mild conditions of emulsion breakage.

The properties of the microgel emulsifier considerably depend on the cross-link density. Dense rigid particles provide higher reduction of interfacial tension, while loosely cross-linked particles are known to be better emulsion stabilizers.^{4,11,13} To all appearances, this is due to the higher lateral overlapping of soft easily deformed microgels, which are able to form a continuous elastic polymer layer at the droplet interface and prevent the coalescence of emulsion droplets.^{9,11} Incorporation of charged groups into the microgels makes them more swollen in comparison with neutral counterparts due to the osmotic pressure exerted by counterions and results in enhanced emulsion stability. The latter should be attributed to the higher swelling and deformability of polyelectrolyte microgels and electrostatic stabilization of the droplet.^{4,9}

Experimental investigation of adsorption thermodynamics revealed that the microgel combines features inherent in solid colloidal particles and single polymer chains.¹⁶ The adsorption energy of microgels with radii of several hundred nanometers was found to be equal to roughly $10^6 k_B T$, which is typical for the solid particles of similar size producing the Pickering emulsions. Such a large value of energy indicates that the emulsifier was trapped by the interface irreversibly. On the other hand, microgels occupied the interface spontaneously without a considerable free energy barrier resembling the behavior of polymers rather than solid colloidal particles.¹⁷ For this reason the adsorption kinetics of the microgels is much faster than that of the solid colloids.¹⁸

Thus, the microgel-stabilized emulsions differ from the Pickering emulsions and require detailed theoretical comprehension. Understanding of a single microgel behavior at the interface seems to be the first step in this challenging study. As to earlier theoretical studies, recent works dealing with the deformation of soft particles placed on rigid^{19,20} or elastic substrates²¹ have taken into account excess surface free energies as well as the elastic energy contributions, but the particle volume has been assumed to be unchanged. A model aimed at the description of small solid iron oxide nanoparticles with grafted poly(ethylene glycol) chains (spherical brushes) of total diameter up to 30 nm placed at a liquid-liquid interface was developed in ref. 22.

In the present paper, we consider the peculiarities of the swelling of a single polymer microgel placed at the interface of two immiscible liquids within a model proposed by us earlier.²³ The theoretical analysis is supported by computer simulations. Our theory takes into account both the microgel deformability and penetrability for both liquids. We examine the microgel spreading at the interface and calculate the interfacial tension inside and outside the microgel. Increasing liquid miscibility

within the polymer particle is predicted. Effects of the solvent quality, microgel size and cross-link density on the anisotropy of swelling are studied.

2 Theoretical model

We consider a polymer microgel placed at the interface of two immiscible liquids denoted as A and B. The amount of liquids is infinite (the thermodynamic limit), and their phase boundary is flat. For the sake of simplicity, the case of symmetrical systems is considered, *i.e.*, A and B molecules interact with the polymer chains evenly. Owing to this symmetry, the center of mass of the microgel lies in the interface plane which divides the microgel into two equal parts. Otherwise, the center of mass is shifted from this plane to a liquid which is a better solvent for the microgel.^{22,23}

The microgel comprises ν subchains, each containing N statistical segments of the length a . In the reference state, the subchains are ideal Gaussian coils of the polymer volume fraction ψ_0 and the radius of the microgel of the spherical shape is determined as $R_0 = (3N\nu/4\pi\psi_0)^{1/3}$ (hereinafter all geometrical dimensions are given in a units); microgel volume in this state is denoted by V_0 .

The exact shape of the deformed microgel at the interface depends on the density and distribution of cross-links as well as on the value of A-B interfacial tension and the particle size.¹⁶ In our model, the microgel is assumed to be uniformly cross-linked and the existence of dangling chains is omitted. Thus, one can reasonably propose that the microgel undergoes affine anisotropic deformation at the A-B interface: its shape can be approximated by an ellipsoid (spheroid) with two equal lateral semi-axes of length $\alpha_r R_0$, and the third semi-axis of length $\alpha_z R_0$ is normal to the phase boundary (Fig. 1). Here α_r and α_z are lateral and normal swelling ratios, respectively. The polymer volume fraction inside the deformed microgel is given by $\psi = \psi_0/\alpha_r^2\alpha_z$ and independent of the spatial coordinates due to the affinity of deformation (*i.e.* uniform swelling). The volume of the microgel and the covered area of the interface are given by $V_{\text{mg}} = N\nu/\psi$ and $S_{\text{surf}} = \pi\alpha_r^2 R_0^2$, respectively.

In order to analyse the microgel swelling and possible flattening, we minimize the Helmholtz free energy of the system F_{tot} . In the following consideration, the free energy and its contributions are expressed in $k_B T$ units, k_B and T being the Boltzmann constant and the absolute temperature, respectively. The free energy can be written as a sum of three terms responsible for the (i) subchain elasticity, (ii) short-range interactions and (iii) excess interfacial free energy, respectively:

$$F_{\text{tot}} = F_{\text{el}} + F_{\text{vol}} + F_{\text{surf}} \quad (1)$$

The elastic free energy of the anisotropically deformed microgel reads

$$F_{\text{el}} = \nu \left[\frac{\alpha_r^2}{3} - \frac{2}{3} N \ln \left(1 - \frac{\alpha_r^2}{N} \right) + \frac{\alpha_z^2}{6} - \frac{1}{3} N \ln \left(1 - \frac{\alpha_r^2}{N} \right) \right] + \nu \left[\frac{1}{\alpha_r^2} + \frac{1}{2\alpha_z^2} \right] \quad (2)$$

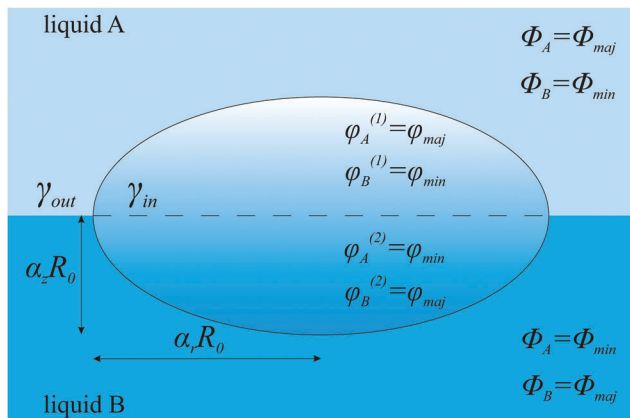


Fig. 1 Schematic representation of the microgel at the interface of two liquids.

Here the first term in the square brackets, accounting for the entropy loss under subchain stretching, is written as an accurate analytical approximation of the inverse Langevin function.^{24,25} It takes into consideration that subchain elongation is restricted by its contour length N , *i.e.* each swelling ratio, α_r and α_z , does not exceed \sqrt{N} . At small elongations ($\alpha_i \ll \sqrt{N}$, $i = r, z$) this expression reproduces well-known results $\nu[\alpha_r^2 + \alpha_z^2/2]$ for the Gaussian elasticity of polymer networks. The second term in eqn (2) corresponds to a reduction of the number of available conformations of the subchains under microgel compression (collapse).^{26,27}

The surface and the volume terms of the total free energy F_{tot} are written in the framework of the Flory–Huggins (FH) lattice theory.^{26–28} Though a number of more sophisticated theoretical models aimed at the consideration of liquid phase equilibrium have been developed,^{29–32} we use the FH theory because of its clarity and the fewest number of numerical parameters. Despite its simplicity, the FH lattice theory properly predicts the behavior of both LCST and UCST polymers if the appropriate dependence of the FH interaction parameter χ_{AP} on temperature T is taken into account.³³ The FH interaction parameter is the function of the free energy change Δf in the process of transfer of a polymer unit from the polymer to the solvent, $\chi_{\text{AP}} = \Delta f/2k_{\text{B}}T$, which in turn contains enthalpy and entropy contributions, $\Delta f = \Delta h - T\Delta s$. For water and polymers containing hydrophobic groups (*e.g.* pNiPAM) both entropy and enthalpy changes in this process are negative, $\Delta h < 0$ and $\Delta s < 0$, since these groups are surrounded by water molecules ordered in the ice-type structure called the clathrate cage. Thus, $\chi_{\text{AP}}(T)$ is found to be an increasing function, and the polymer reveals LCST behavior (pNiPAM-based gel collapses under heating). If polymer units are capable of hydrogen bonding with each other, the polymer dissolution is accompanied by breaking of these bonds so that $\Delta h > 0$ and $\Delta s > 0$. These polymers, for instance copolymers of poly(acrylamide) and poly(acrylic acid), reveal UCST behavior.³³ Since the aim of this paper is the development of a general theory, we calculate the equilibrium characteristics of the system as a function of the FH interaction parameters. In order to pass from the theoretical χ -dependencies to the T -dependencies which can be observed

experimentally, one should additionally introduce $\chi(T)$ relation specific for each polymer/solvent pair.

The microgel interior and outer solution are considered as ternary and binary mixtures, respectively, and the free energy densities of short-range interactions in these regions, f_{in} and f_{out} , take the following forms:

$$f_{\text{in}} = \phi_{\text{A}} \ln \phi_{\text{A}} + (1 - \psi - \phi_{\text{A}}) \ln(1 - \psi - \phi_{\text{A}}) + \chi_{\text{AB}} \phi_{\text{A}} (1 - \psi - \phi_{\text{A}}) - \chi_{\text{AP}} (1 - \psi)^2; \quad (3)$$

$$f_{\text{out}} = \Phi_{\text{A}} \ln \Phi_{\text{A}} + (1 - \Phi_{\text{A}}) \ln(1 - \Phi_{\text{A}}) + \chi_{\text{AB}} \Phi_{\text{A}} (1 - \Phi_{\text{A}}) - \chi_{\text{AP}}. \quad (4)$$

Here ϕ_{A} and Φ_{A} are the volume fractions of the solvent A inside and outside the microgel, respectively. The FH interaction parameter between A and B molecules is denoted as χ_{AB} , and χ_{AP} is the one corresponding to the contacts between the polymer segment and the molecules of the A and B liquids (owing to the symmetry of the system $\chi_{\text{AP}} = \chi_{\text{BP}}$). Note that the free energy of short-range interactions

$$F_{\text{vol}} = V_{\text{mg}}(f_{\text{in}} - f_{\text{out}}) = \frac{N\nu}{\psi}(f_{\text{in}} - f_{\text{out}}) \quad (5)$$

as well as the elastic free energy are linear functions of the parameter ν .

It is well known that a homogeneous mixture of two immiscible liquids of the symmetric (1:1) composition becomes unstable and separates into two coexisting phases as soon as χ_{AB} exceeds the critical value, $\chi_{\text{AB}}^{\text{cr}} = 2$. Volume fractions of the liquid A in these phases, $\Phi_{\text{maj}} > 1/2$ and $\Phi_{\text{min}} < 1/2$, are determined by the equality of the chemical potentials and the pressures (see Fig. 2, black curve):

$$\mu_{\text{out}} = \left. \frac{df_{\text{out}}}{d\Phi_{\text{A}}} \right|_{\Phi_{\text{A}}=\Phi_{\text{min}}} = \left. \frac{df_{\text{out}}}{d\Phi_{\text{A}}} \right|_{\Phi_{\text{A}}=\Phi_{\text{maj}}}; \quad (6)$$

$$\begin{aligned} \Pi_{\text{out}} &= \left(\Phi_{\text{A}} \frac{df_{\text{out}}}{d\Phi_{\text{A}}} - f_{\text{out}} \right) \Big|_{\Phi_{\text{A}}=\Phi_{\text{min}}} \\ &= \left(\Phi_{\text{A}} \frac{df_{\text{out}}}{d\Phi_{\text{A}}} - f_{\text{out}} \right) \Big|_{\Phi_{\text{A}}=\Phi_{\text{maj}}} \end{aligned} \quad (7)$$

Relationship $\Phi_{\text{maj}} + \Phi_{\text{min}} = 1$ is a consequence of the symmetry of the system including equal volumes of A and B molecules, each occupying one lattice site. To find the values of Φ_{maj} and Φ_{min} , eqn (6) and (7) have to be solved numerically. The FH parameter χ_{AB} is a measure of liquid immiscibility: the higher the value of χ_{AB} , the closer the value of Φ_{maj} to unity and Φ_{min} to zero (Fig. 2). Finally, dimensionless surface tension between these phases expressed in $k_{\text{B}}T/a^2$ units³⁴

$$\gamma_{\text{out}} = 2\sqrt{\chi_{\text{AB}}} \int_{\Phi_{\text{min}}}^{\Phi_{\text{maj}}} d\Phi_{\text{A}} \sqrt{f_{\text{out}}(\Phi_{\text{A}}) - \mu_{\text{out}}\Phi_{\text{A}} + \Pi_{\text{out}}} \quad (8)$$

depends solely on χ_{AB} and increases as χ_{AB} increases.

A mixture of A and B liquids within the polymer particle at $\chi_{\text{AB}} > 2$ is either homogeneous, with volume fractions $\phi_{\text{A}} = \phi_{\text{B}} = (1 - \psi)/2$, or separated. In the latter case each (micro)phase takes up a half of the microgel, and these (micro)phases are

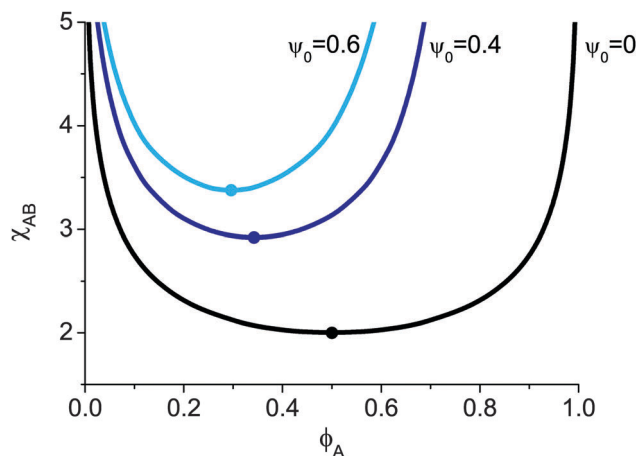


Fig. 2 Theoretical binodals of the mixture of A and B liquids outside the gel ($\psi_0 = 0$) and within it for different values of the polymer volume fraction in the reference state: $\psi_0 = 0.6$ and $\psi_0 = 0.4$. $N = 5$ and $\chi_{AP} = 0$ (both liquids are very good solvents for the gel). The critical point in each curve is depicted by a bold dot.

symmetric, *i.e.* volume fractions of A and B liquids in foreign (micro)phases are equal:

$$\phi_A^{(1)} = \phi_B^{(2)} = \phi_{\text{maj}}; \quad (9)$$

$$\phi_A^{(2)} = \phi_B^{(1)} = \phi_{\text{min}}; \quad (10)$$

$$\phi_{\text{maj}} + \phi_{\text{min}} + \psi = 1. \quad (11)$$

The last relationship expresses a space-filling condition. Similar to the case of outer solution, the values of ϕ_{maj} and ϕ_{min} fulfil conditions

$$\mu_{\text{in}} = \left. \frac{df_{\text{in}}}{d\phi_A} \right|_{\phi_A=\phi_{\text{min}}} = \left. \frac{df_{\text{in}}}{d\phi_A} \right|_{\phi_A=\phi_{\text{maj}}}; \quad (12)$$

$$\Pi_{\text{in}} = \left(\phi_A \frac{df_{\text{in}}}{d\phi_A} - f_{\text{in}} \right) \Big|_{\phi_A=\phi_{\text{min}}} = \left(\phi_A \frac{df_{\text{in}}}{d\phi_A} - f_{\text{in}} \right) \Big|_{\phi_A=\phi_{\text{maj}}} \quad (13)$$

and the dimensionless interfacial tension at the A–B interface within the microgel given by

$$\gamma_{\text{in}} = 2\sqrt{\chi_{AB}} \int_{\phi_{\text{min}}}^{\phi_{\text{maj}}} d\phi_A \sqrt{f_{\text{in}}(\phi_A, \psi) - \mu_{\text{in}}\phi_A + \Pi_{\text{in}}} \quad (14)$$

is a function of both χ_{AB} and the polymer volume fraction inside the microgel, ψ . The interfacial tension within the microgel is always lower than out of it, $\gamma_{\text{out}} > \gamma_{\text{in}}$. In subsequent calculations numerical parameters are chosen in such a way so that the microgel thickness $2\alpha_z R_0$ exceeds by far the thickness of the phase boundary inside the microgel, and eqn (12)–(14) are applicable.

Because both liquids are considered to be equally good solvents for the microgel, $\chi_{AP} \leq 1/2$, there is no excess surface free energy on the outer surface of the microgel. Hence, the surface term F_{surf} is directly proportional to the surface area

S_{surf} of the liquid–liquid interface which is covered by the microgel:

$$F_{\text{surf}} = S_{\text{surf}}(\gamma_{\text{in}} - \gamma_{\text{out}}) = \pi\alpha_r^2 \left(\frac{3N\nu}{4\pi\psi_0} \right)^{2/3} (\gamma_{\text{in}} - \gamma_{\text{out}}) \quad (15)$$

Excess free energy F_{lin} at the triple boundary line (liquid A–liquid B–microgel) is disregarded since it is negligible as compared to the surface term, F_{surf} . Indeed, F_{lin} is proportional to the line tension κ and the line length which is of the order of microgel dimensions, $F_{\text{lin}} \sim R_0\kappa$, while the line tension is related to the surface tension via $\kappa \sim a\gamma$. Thus, the ratio $F_{\text{lin}}/F_{\text{surf}} \sim a/R_0$ is much lower than unity owing to the microgel dimensions which exceed by far the specific microscopic length of the system, $R_0 \gg a$.

The equilibrium free energy of the system is calculated numerically *via* minimization of F_{tot} with respect to the linear swelling ratios α_r and α_z . In doing so, we take into account that both the volume fractions ϕ_{min} , ϕ_{maj} and the surface tension γ_{in} depend on α_r and α_z .

3 Computer simulations

Dissipative particle dynamics (DPD) computer simulations of microgel swelling in the bulk (if A and B liquids form a homogeneous mixture) and at the interface of the two liquids (if they are segregated) were performed. Details on the design of the spherical microgel can be found in ref. 18 and 35–37. In brief, fully stretched subchains (each of M beads) were connected through tetrafunctional junctions and repeated a unit cell of the diamond crystal lattice. Then, we constructed a cubic frame out of the unit cells. To provide a ‘spherical’ shape of the microgel, we inscribed a sphere into the frame and ‘cropped’ all the beads that were outside the sphere. As a result, we obtained a microgel containing both subchains and dangling chains. The number of subchains ν and their length M varied. The simulations were performed in a cubic box with imposed periodic boundary conditions in all coordinates. The linear sizes of the box were taken as $L_x = L_y = L_z = 60$ expressed in units of bead diameter. The density of the system was chosen to be $\rho = \mathcal{N}/V = 3$ so that the total number of beads of all types in the box was $\mathcal{N} = 3 \times 60^3$. The composition of A and B liquids (beads) was always symmetric (1 : 1). For any beads of the i th type, the DPD interaction parameter a_{ii} was fixed, $a_{ii} = 25$. The relationship between the DPD interaction parameters a_{ij} , quantifying incompatibility of the beads of different types (liquid–liquid and polymer–liquid), and the corresponding FH interaction parameters is given by^{38,39}

$$\chi_{ij} = (0.286 \pm 0.002) \cdot (a_{ij} - 25) \quad (16)$$

The parameter a_{AB} was varied between 25 and 60 that accords with the χ_{AB} -range from 0 to 10. As in the theoretical treatment, only the symmetric case is studied in the DPD simulations, $a_{AP} = a_{BP}$. However, the obtained principal results on microgel conformations and miscibility of the liquids inside it remain valid in the case of small asymmetry as well. At that, better quality of one of the solvents leads to the deeper immersion of the microgel

into this liquid (see ref. 23 for details). Though solvent quality of a couple of immiscible liquids for polymer microgels is hardly exactly the same, it can be approximately equal. *E.g.* water and low polar oil toluene are highly immiscible (solubility of toluene in water is low, 0.52 g l^{-1} at 20°C) but both are known to be good solvents for poly(*N*-vinylcaprolactam).⁴⁰

In order to characterize the microgel shape and dimensions, lateral, R_r , and normal (with respect to the plane of the interface), R_z , components of the gyration radius were calculated:

$$R_r^2 = \frac{1}{2P^2} \sum_{i,j=1\dots P} \langle (x_i - x_j)^2 + (y_i - y_j)^2 \rangle \quad (17)$$

$$R_z^2 = \frac{1}{2P^2} \sum_{i,j=1\dots P} \langle (z_i - z_j)^2 \rangle \quad (18)$$

Here, P is the total number of beads in the microgel. The Cartesian axes x and y are chosen to be in the plane of the interface and the z -axis is normal to the plane. The angle brackets denote the averaging. The corresponding components in a pure A (or B) liquid are denoted with index 0, R_r^0 and R_z^0 .

4 Results and discussion

In the total free energy of the system, the elastic, F_{el} , and the volume, F_{vol} , contributions are proportional to the number of subchains ν , while the surface term, F_{surf} , depends on $\nu^{2/3}$. Therefore, if we consider a macroscopic gel, $\nu \rightarrow \infty$, the surface effects are negligible and F_{surf} can be omitted. We start our analysis with the macroscopic gel (so-called volume approximation) and then pass to relatively small polymer microgels.

4.1 Swelling of a macroscopic gel in a mixture of two liquids

Let us consider a polymer gel which is immersed into an excess amount of A and B liquids. Since surface effects are disregarded, the gel swelling is uniform: $\alpha_r = \alpha_z = (\psi_0/\psi)^{1/3}$. Minimization of the free energy allows us to plot binodals of the system (Fig. 2). Certainly, this approach is equivalent to the conventional consideration of the equilibrium of four phases: A and B liquids outside the gel, and two phases enriched by A and B liquids inside the gel. Eqn (6), (7) and (12), (13) should be solved together with the following relationships, reflecting the equality of chemical potentials and (osmotic) pressures inside and outside the gel:⁴¹

$$\mu_{in} = \mu_{out} \quad (19)$$

$$\Pi_{in} + \psi \frac{d}{d\psi} \left(f_{in} + \frac{F_{el}}{V_{mg}} \right) - \frac{F_{el}}{V_{mg}} = \Pi_{out} \quad (20)$$

The different curves in Fig. 2 correspond to the different values of the polymer volume fraction ψ_0 in the reference state, $\psi_0 = 0.6$ and $\psi_0 = 0.4$, *i.e.* the gels have equal length and flexibility of the subchains but different excluded volumes of monomer units. The black curve corresponds to the mixture of liquids outside the gel, $\psi_0 = 0$. Coordinates of the critical point in this case are equal to $\Phi_A^{cr} = 1/2$ and $\chi_{AB}^{cr} = 2$. Two other curves

show that the miscibility of the liquids inside the gel increases and phase separation takes place at considerably higher values of χ_{AB} . For instance, the mixture of A and B liquids with $\chi_{AB} = 3$ splits into two phases outside the gel, while the mixture remains homogeneous inside the gel with $\psi_0 = 0.6$ (Fig. 2). In general, the denser the gel, the better the miscibility of the liquids within it.

To find coordinates of the critical point in this symmetric system, it is necessary to solve the following equations:

$$\begin{cases} \frac{d^2}{d\phi_A^2}(F_{el} + F_{vol}) = 0 \\ \frac{d^3}{d\phi_A^3}(F_{el} + F_{vol}) = 0 \\ \frac{d}{d\psi}(F_{el} + F_{vol}) = 0 \end{cases} \quad (21)$$

The first and the second equations allow getting analytical formulae connecting coordinates of the critical point:

$$\phi_A^{cr} = \frac{1 - \psi}{2} \quad \chi_{AB}^{cr} = \frac{2}{1 - \psi} \quad (22)$$

Note that this result does not depend on the solvent quality, *i.e.* on χ_{AP} , and remains valid for poor solvent ($\chi_{AP} > 0.5$) as well. The derived value of ϕ_A^{cr} is a direct consequence of the symmetry of the system. The expression defining χ_{AB}^{cr} shows that the increase of polymer volume fraction inside the gel promotes the miscibility of the liquids. Finally, the equilibrium value of ψ , which is a measure of the gel swelling, was found by numerical solution of the third equation in the system (21) with conditions (22). The enhanced miscibility of the liquids within the gel is explained²³ by a shielding of unfavorable contacts between A and B molecules by monomer units of the gel: the larger the concentration of the monomer units (ψ), the better the miscibility.

The equilibrium volume of the swollen gel (volume swelling coefficient), V_{gel}/V_0 , and the polymer volume fraction within the gel, ψ , are presented in Fig. 3 as a function of χ_{AB} . Both the functions are nonmonotonous. The molecules of A and B types are indistinguishable at $\chi_{AB} = 0$, and the gel volume is equal to one in pure A (or pure B) liquid. The ratio V_{gel}/V_0 exceeds unity because of the volume interactions: $\chi_{AP} = 0$ corresponds to the good solvent conditions. At that, higher swelling of the gel with bulkier monomer units ($\psi_0 = 0.6$) with respect to the reference state, where the subchains are Gaussian coils, is a consequence of their stronger steric repulsion. On the contrary, strong segregation of the liquids occurs inside the gel at very high immiscibility of the liquids, $\chi_{AB} \gg 1$, and the coexisting phases are practically pure. It means that half of the gel swells in almost pure A liquid and another half in almost pure B liquid. Therefore, the swelling coefficients of the gel have to be equal at $\chi_{AB} = 0$ and $\chi_{AB} \rightarrow \infty$. It is clearly seen in Fig. 3a that the gel volumes at $\chi_{AB} = 0$ and $\chi_{AB} = 10$ are already very close to each other.

Extra swelling of the gel at $0 < \chi_{AB} < 2$ is related to homogeneous mixing of the liquids outside the gel. Such mixing is accompanied by gain in the entropy and penalty in

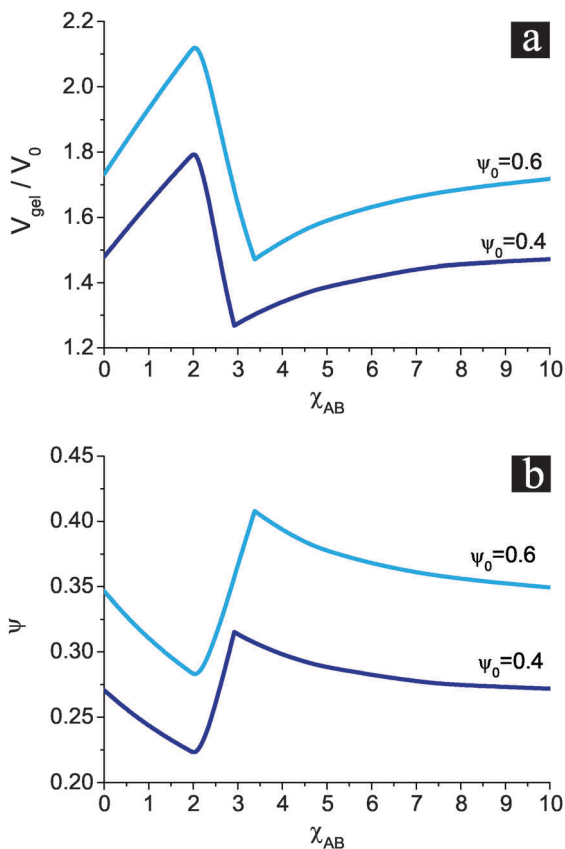


Fig. 3 Theory. Dimensionless volume of the swollen gel, V_{gel}/V_0 (volume swelling coefficient) (a), and polymer volume fraction ψ inside the gel (b) as a function of χ_{AB} at different values of the polymer volume fraction in the reference state, $\psi_0 = 0.6$ and 0.4 ; $N = 5$, $\chi_{AP} = 0$.

the energy: there are plenty of unfavorable contacts between A and B molecules in the homogeneous mixture. As an alternative, the energy can be reduced if some of the A and B molecules will enter the gel where the number of unfavorable contacts will be reduced by the monomer units of the gel. Thus, the gel swells. In the range $2 < \chi_{AB} < \chi_{AB}^{\text{ct}}$, the outer solution undergoes phase separation, but the mixture remains homogeneous inside the gel (Fig. 2).^{41,42} The gel shrinkage with χ_{AB} is driven by ‘optimization’ of the energy of the system as well. Despite a partial shielding of unfavorable contacts between A and B molecules in the gel by the monomer units, the number of contacts is large enough and increasing χ_{AB} leads to a considerable increase of the energy. On the other hand, the number of A–B contacts outside the gel is minimum because of the phase separation. Therefore, escape of some of the A and B molecules from the gel and their segregation outside the gel is energetically favorable. This escape and gel shrinkage stops when the increasing fraction of monomer units provides enough shielding of the A–B contacts. Finally, further gel swelling at $\chi_{AB} > \chi_{AB}^{\text{ct}}$ is related to the segregation of the liquids both outside and inside the gel. Segregation of A and B molecules in combination with the shielding effect of monomer units allows the entry of some of the A and B molecules into the gel without essential penalty in the energy.

The limiting swelling degree at $\chi_{AB} \rightarrow \infty$ is equivalent to the swelling in one-component solvent.

4.2 Swelling of a microgel at the liquid–liquid interface

In this case we have to consider the surface effects taking into account the interfacial free energy term, F_{surf} . The binodal of the symmetric mixture of the liquids inside the microgel is shown in Fig. 4. The increase of χ_{AB} induces abrupt rather than gradual (micro)phase separation of the liquids inside the microgel. In other words, the homogeneous AB mixture segregates at once into two (micro)phases with a finite difference in concentrations of coexisting phases, $\phi_A^{(1)} - \phi_A^{(2)}$, while in the macroscopic gel $\phi_A^{(1)} - \phi_A^{(2)} = (\phi_{\text{maj}} - \phi_{\text{min}}) \rightarrow 0$ continuously at $\chi_{AB} \rightarrow \chi_{AB}^{\text{ct}}$. This result is caused by the finite size of the system and can be clarified as follows. In the macroscopic gel ($\nu \rightarrow \infty$), the phase separation is described by the volume contributions $\sim \nu$. The appearance of an additional positive term in the free energy of the microgel, $F_{\text{surf}} \sim \nu^{2/3}$, is responsible for the additional penalty of the free energy in the separated liquids: the formation of the interface in the finite-size object costs more energy than in the infinite one. In other words, one needs to spend more energy in order to induce phase separation in the finite size object. Therefore, the transition to the separated state in the microgel is ‘delayed’, *i.e.* shifted towards higher values of χ_{AB} , and occurs in a jump-like manner. Though it is well known that the FH theory is a mean-field theory and fails to properly predict critical behavior and values of the critical exponents,⁴³ the character of phase transitions between homogeneous and separated states of the liquids is described correctly within the theory. The transitions inside and outside the microgel are discontinuous and continuous, respectively.

Dependencies of the interfacial tension inside and outside the microgel on χ_{AB} are shown in Fig. 5. As long as the mixture is homogeneous, the corresponding tensions are equal to zero. The interfacial tension outside the microgel gradually increases with χ_{AB} from 0 at the critical point, $\chi_{AB}^{\text{ct}} = 2$. In contrast, γ_{in} jumps from zero to some small value at the binodal, $\chi_{AB}^{\text{bin}} = 3.51$ (see Fig. 5, inset), and increases further with χ_{AB} continuously.

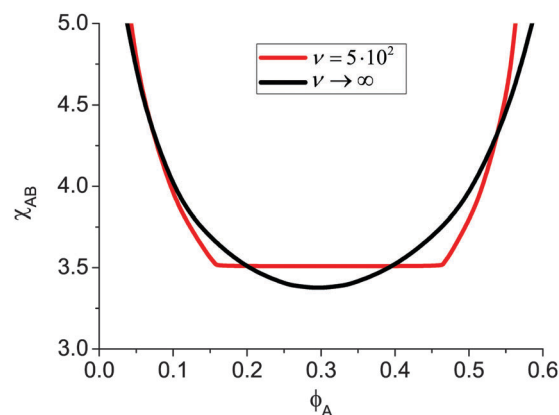


Fig. 4 Theoretical binodals of the mixture of A and B liquids within the microgel ($\nu = 5 \times 10^2$, red curve) and the macroscopic gel ($\nu \rightarrow \infty$, black curve) at $\psi_0 = 0.6$, $N = 5$ and $\chi_{AP} = 0$.

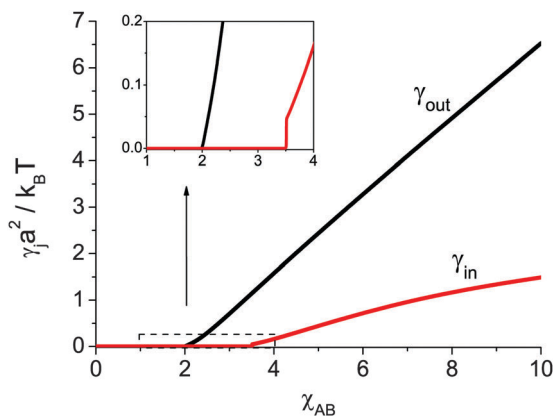


Fig. 5 Theoretical interfacial tensions within the microgel γ_{in} (red curve) and out of it γ_{out} (black curve) at $\psi_0 = 0.6$, $N = 5$ and $\chi_{AP} = 0$. Inset is a zoom of the rectangular area and demonstrates continuous and abrupt growth of the interfacial tension outside and inside the microgel, respectively.

The jump of γ_{in} is related to the abrupt separation of the liquids within the microgel at $\chi_{AB}^{bin} = 3.51$. Fig. 5 demonstrates that the interfacial tension of segregated liquids is always higher outside the microgel than inside. This fact reveals the surface activity of the microgels. We can also see in Fig. 5 that γ_{out} increases faster than γ_{in} . It means that the microgel will be more strongly ‘bound’ to the interface at higher values of χ_{AB} , *i.e.* its adsorption will be accompanied by higher gain in the energy. Also, we can expect that the microgel will flatten at the interface with the increase of χ_{AB} to occupy as large an area as possible to minimize the total interfacial energy.

The microgel deformation at the interface is clearly seen in computer simulations (Fig. 6).

Different snapshots correspond to different values of the DPD interaction parameter a_{AB} which quantifies the incompatibility of the liquids. This parameter ranges from $a_{AB} = 34$ to $a_{AB} = 60$, which accords with the range of the FH interaction parameter $2.574 \leq \chi_{AB} \leq 10.01$. The higher the liquid immiscibility, the stronger the microgel flattening. The value $a_{AB} = 34$ corresponding to $\chi_{AB} = 2.574$ is high enough to provide phase separation of liquids in the outer solution (Fig. 6). The DPD interaction parameters between the polymer and liquid beads, $a_{AP} = a_{BP} = 25$, corresponded to a good solvent for microgel subchains, $\chi_{AP} = \chi_{BP} = 0$. Some snapshots depict microgel protrudes into one phase slightly more than another despite A and B molecules interact with the polymer evenly. This should

be attributed to the thermal fluctuations of the microgel, because the snapshots correspond to momentary rather than averaged microgel location and shape. At the same time, the snapshots show that the ellipsoidal microgel shape is appropriate theoretical assumption if immiscibility of the liquids is not too high. Deviations from the ellipsoidal shape are primarily caused by dangling chains at the particle edges (Fig. 6, $a_{AB} = 60$) occupying extra interfacial area almost without penalty in the elastic free energy. At very high values of χ_{AB} and low cross-link densities, the microgel shape resembles pancake rather than ellipsoid.¹⁸

Effects of (i) microgel dimensions, (ii) cross-link density and (iii) solvent quality for polymer subchains on microgel swelling, deformation as well as A and B liquid miscibility within the particle are studied below (subsections A, B and C, respectively).

A Effect of the microgel size. The effect of the microgel size on its spreading over the interface and anisotropy of swelling is presented in Fig. 7. In the range $0 < \chi_{AB} < 2$, two liquids are homogeneously mixed and the microgel adopts a spherical shape in the solution, *i.e.* $\alpha_r = \alpha_z$, and the degree of swelling does not depend on the number of subchains ν . The results of the volume approximation are exactly reproduced in this range of χ_{AB} because $\gamma_{in} = \gamma_{out} = 0$ and $F_{surf} = 0$. Both linear swelling ratios, α_r and α_z , are higher than unity at $\chi_{AB} = 0$ owing to the repulsive volume interactions (χ_{AP} corresponds to the good solvent).

Once χ_{AB} exceeds 2, the liquid-liquid interface appears and the adsorbed microgel undergoes flattening ($\alpha_r > \alpha_z$), whereas swelling of the macroscopic gel remains isotropic, $\alpha_r = \alpha_z$ at $\nu \rightarrow \infty$. The smaller the microgel, the higher the ratio α_r/α_z defining the swelling anisotropy. For the smallest microgel with $\nu = 500$ (Fig. 7), the interfacial area covered by the microgel, S_{surf} , at high χ_{AB} is almost twice larger than the cross-section of the microgel in pure A (or B) liquid ($\chi_{AB} = 0$), though the subchains are rather short, $N = 5$. The decrease in the normal swelling ratio α_z compensates the increase of α_r , so that the polymer volume fraction inside the microgel changes moderately.

The value of ν at which the microgel starts to undergo a well-pronounced flattening can be estimated analytically. Excess surface free energy provoking microgel deformation reads

$$F_{surf} = \pi\alpha_r^2 R_0^2 (\gamma_{in} - \gamma_{out}) \simeq -\pi\alpha_r^2 \left(\frac{3N\nu}{4\pi\psi_0} \right)^{2/3} (\gamma_{out} - \gamma_{in}) \quad (23)$$

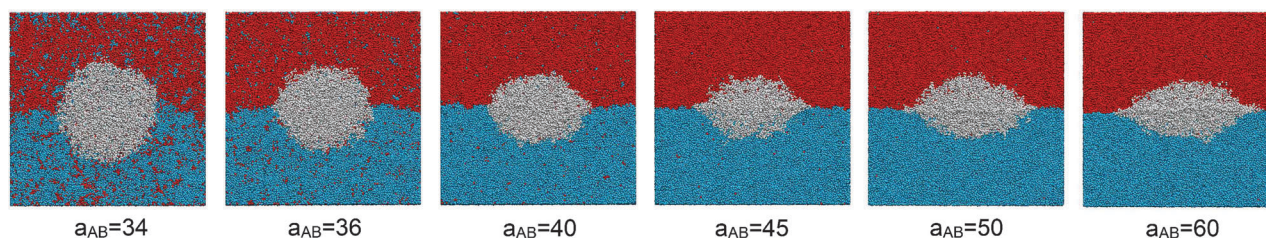


Fig. 6 Computer simulation snapshots of the polymer microgel consisting of $\nu = 2428$ subchains, each of the length $M = 5$, at the interface of A and B liquids; $a_{AP} = a_{BP} = 25$, a_{AB} ranges from 34 to 60.

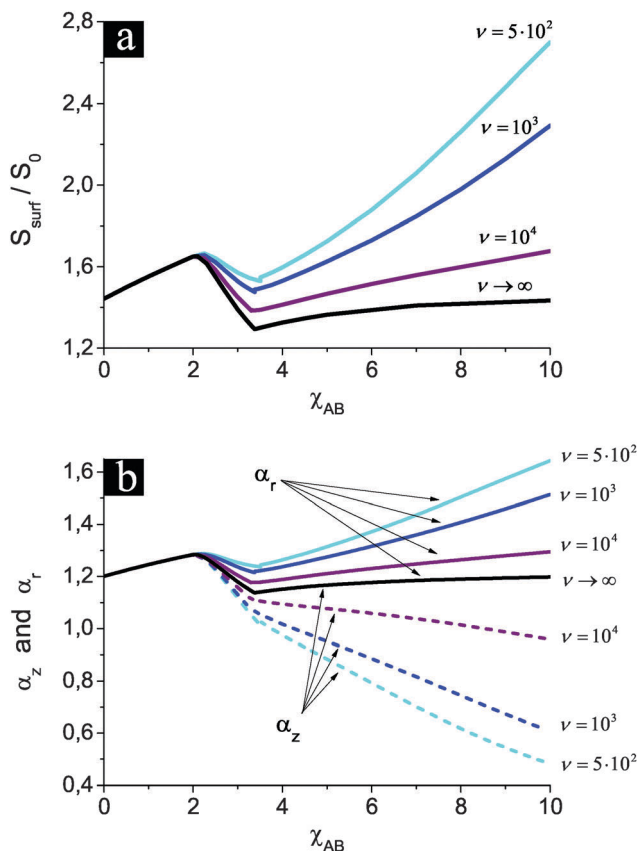


Fig. 7 Theory. (a) The ratio of the interfacial area occupied by the microgel S_{surf} to the area of cross-section S_0 of the spherical microgel swollen in the homogeneous mixture, S_{surf}/S_0 , and (b) the radial, α_r (solid line), and the normal, α_z (dashed line), swelling ratios of the microgel versus χ_{AB} at $\psi_0 = 0.6$, $N = 5$, and $\chi_{AP} = 0$. The curves correspond to the microgels of different numbers of subchains: $\nu = 5 \times 10^2$, 10^3 and 10^4 . Black curves represent the case of the macroscopic gel, $\nu \rightarrow \infty$.

while the free energy of the microgel stretching in the limit of low deformations is given by the Gaussian approximation

$$F_{\text{el}} \simeq \nu \alpha_r^2. \quad (24)$$

Both these terms depend on the radial swelling ratio in the same manner: they are proportional to α_r^2 . Flattening of the microgel occurs if the surface tension overcomes the elastic contribution which gives the following criterion:

$$\nu \lesssim \nu^*, \quad \nu^* = \frac{9\pi N^2 (\gamma_{\text{out}} - \gamma_{\text{in}})^3}{16 \psi_0^2} \quad (25)$$

Thus, only small enough microgels undergo flattening. Since in the reference state ψ_0 depends not only on the structure of the monomer unit but also on the subchain length as $\psi_0 \sim 1/\sqrt{N}$, we get $\nu^* \sim N^3$. Virtually the dependence of ν^* on N is slightly weaker and the exponent is a bit lower than 3 because loosely cross-linked microgels are less capable of enhancing liquid miscibility and reducing interfacial tension inside itself (see Fig. 9 below, γ_{in} is an increasing function of N). Notably, the

dependence of ν^* on N is so strong, *i.e.* microgel cross-linking density is a crucial factor affecting microgel flattening.

Unfortunately, the value of the inner surface tension γ_{in} cannot be expressed analytically at a given χ_{AB} , and it is difficult to obtain the precise estimation of the microgel size ν^* . To avoid this difficulty, let us adopt the following assumption

$$\gamma_{\text{out}} - \gamma_{\text{in}} \simeq \gamma_{\text{out}} [1 - (1 - \psi)^2] \quad (26)$$

supported by our calculations of the surface tensions (see Fig. 5) and which is reasonable in the strong segregation approximation ($\chi_{AB} \gg 1$) when $\gamma_{\text{out}} \simeq \pi \chi_{AB}/4$ and $\gamma_{\text{in}} \simeq \pi(1 - \psi)^2 \chi_{AB}/4$.²³ The value of ψ can be chosen equal to the polymer volume fraction in the microgel swollen in a pure A (or B) liquid. Then we get $\nu^* \simeq 3 \times 10^3$ at $\chi_{AB} = 6$, which is in agreement with exact numerical results, Fig. 7a.

Finally, we would like to note that in the present consideration it is necessary to use the form of the elastic free energy accounting for a finite chain extensibility. Indeed, if we assume the chain elasticity to be Gaussian, one can find that the subchain end-to-end distance exceeds its contour length for the small microgels, $\nu < \nu^*$. In order to avoid this problem, either the Langevin form of the elastic free energy^{35,44,45} or its analytical approximation^{24,25} (eqn (2)) should be adopted.

Swelling of microgels of various sizes was performed in DPD computer simulations. To demonstrate that the microgels of the different sizes swell anisotropically, the components R_r and R_z of the gyration radius were plotted as a function of χ_{AB} (Fig. 8). They can be directly compared with the theoretical swelling ratios α_r and α_z since the microgel was approximated as an ellipsoid (spheroid), with X - and Y -semiaxes equal to $\alpha_r R_0$ and the Z -semiaxis equal to $\alpha_z R_0$. Indeed, the components R_r and R_z of the gyration radius of the spheroid known to be $\sqrt{2} \alpha_r R_0 / \sqrt{5}$ and $\alpha_z R_0 / \sqrt{5}$, respectively, are linear functions of respective microgel semiaxes. Similar to the theoretical calculations, the components of the gyration radius are presented in dimensionless form (Fig. 8).

At $\chi_{AB} < 2$, the microgel swelling in the homogeneous mixture of the liquids is isotropic, $R_r/R_r^0 = R_z/R_z^0$ (Fig. 8). In accordance with the theoretical predictions (Fig. 7a), small microgels undergo stronger flattening at $\chi_{AB} > 2$, and the radial microgel size changes non-monotonically. The larger the microgel, the higher the value of χ_{AB}^{bin} and the broader the range $2 < \chi_{AB} < \chi_{AB}^{\text{bin}}$ where the microgel lateral dimensions diminish. At that, both theory and simulations predict growth of the microgel thickness upon increasing liquid incompatibility until the mixture segregates into two phases within the microgel ($\chi_{AB} = \chi_{AB}^{\text{bin}}$). The lateral dimensions in the vicinity of χ_{AB}^{bin} for large enough microgels can be even lower than ones in a pure A/B liquid (compare Fig. 7 and 8a). In contrast, for the small microgels, the decrease of the covered interfacial area at $2 < \chi_{AB} < \chi_{AB}^{\text{bin}}$ is rather moderate. It is natural that the behavior of small microgels with long subchains resembles the behavior of single chains placed at the A–B interface. They reveal monotonously increasing lateral dimensions with increasing χ_{AB} . A slight difference in the numerical values of

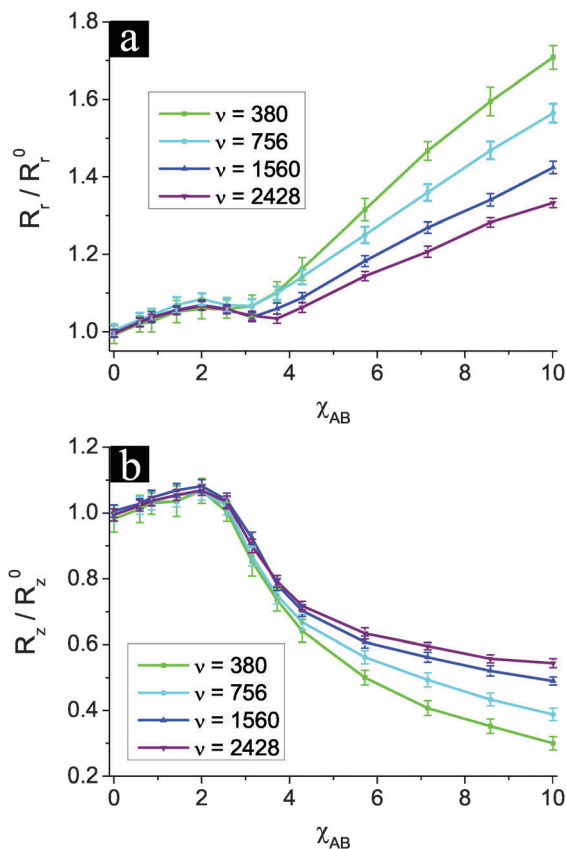


Fig. 8 Computer simulations. Lateral, R_r , and normal, R_z , components of the gyration radius of the microgel adsorbed at the interface as a function of the interaction parameter χ_{AB} . They are normalized to the corresponding components in pure A (or B) liquids, R_r^0 and R_z^0 . The curves are plotted for the microgels of different sizes: $\nu = 380, 756, 1560$, and 2428 . The parameters $M = 10$ and $\chi_{AP} = \chi_{BP} = 0$ (*i.e.* $a_{AP} = a_{BP} = 25$) are fixed.

the swelling ratios and normalized gyration radii (*e.g.* α_r and R_r) should be ascribed to different choices of the reference states. Microgels with the Gaussian subchains in the theory ($\alpha_r = \alpha_z = 1$) and the microgels swollen in a pure A (or B) liquid in simulations (R_r^0 and R_z^0) were adopted to be these states.

It is necessary to note that uniform mixing of the liquids within the microgel at $2 < \chi_{AB} < \chi_{AB}^{\text{bin}}$ has already been confirmed by us in computer simulations,²³ and the corresponding density profiles of the liquids within the microgel can be found below.

B Effect of the microgel cross-link density. Analytical estimates (25) of the parameter ν^* , below which the microgel demonstrates high oblateness at the interface, reveal that the cross-link density is one of the crucial factors controlling the microgel behavior. To explore more thoroughly the influence of the cross-link density on the microgel shape, its surface activity and ability to mix liquids, we plot a set of curves corresponding to the microgels of various subchain lengths, $N = 5, 7$ and 10 (Fig. 9). Different microgels have equal dry mass, $N\nu = 5 \times 10^4$; the polymer volume fraction in the reference state depends on the subchain length, $\psi_0 \sim 1/\sqrt{N}$. Decreasing cross-link density (increasing N) results in stronger flattening of the microgel

(Fig. 9a and b) and higher anisotropy of the swelling (Fig. 9d), which is defined by the aspect ratio of an oblate spheroid, α_r/α_z . Irrespective of the subchain length N , the swelling of the microgel becomes non-uniform exactly at $\chi_{AB} = 2$ (Fig. 9d), *i.e.* as soon as phase separation in the outer solution occurs and the interface is formed. Below the critical point, it is expectable that the lateral and normal swelling ratios are equal $\alpha_r = \alpha_z$. In pure A (or B) liquid ($\chi_{AB} = 0$) higher swelling of loosely cross-linked microgels is due to the fact that both liquids are good solvents for the subchains, $\chi_{AP} = \chi_{BP} = 0$. Densely cross-linked microgels promote liquid miscibility and lower interfacial tension stronger than the weakly cross-linked microgels (Fig. 9e and f, respectively).

It is necessary to stress that the dependence of the polymer volume fraction within the microgel ψ on χ_{AB} differs from that for the macroscopic gel in the region of high χ_{AB} (compare Fig. 3b and 9c). Shrinkage of the microgel at high immiscibility of the liquids diminishes the number of A–B contacts within the microgel and lowers the surface tension inside it. The shrinkage is higher for the loosely cross-linked microgel, $N = 10$, because low polymer density within it results in a higher excess surface free energy. Contraction of the macroscopic gel is absent in the region of high χ_{AB} since surface effects are negligible.

The theoretical results are supported by computer simulations of microgels with different numbers of beads in each subchain $M = 3, 5$ and 10 . All microgels, albeit cross-linked with different densities, contain approximately equal total numbers of beads: 8039, 8025 and 8049, respectively. The corresponding components of the gyration radius *vs.* χ_{AB} are shown in Fig. 10.

For any value of the subchain length M , R_r demonstrates non-monotonous behaviour. As predicted theoretically (Fig. 9a), it increases up to $\chi_{AB} = 2$, then decreases in the range $2 < \chi_{AB} < \chi_{AB}^{\text{bin}}$ (inset in Fig. 10a), and increases again as χ_{AB} exceeds χ_{AB}^{bin} . The shift of χ_{AB}^{bin} for denser microgels towards higher values is also observed in the inset of Fig. 10a.

In accordance with the theoretical predictions, loosely cross-linked particles undergo stronger flattening than densely cross-linked ones. Stronger decay of the microgel thickness takes place in loosely cross-linked microgels, compare Fig. 10b (simulations) and Fig. 9b (theory).

Theoretically predicted slight microgel shrinkage (*i.e.* increase of ψ) in the region of high χ_{AB} is not confirmed by simulations if one calculates the microgel volume as the volume of ellipsoid, $V_{\text{mg}} = 4\pi R_r^2 R_z/3$. This discrepancy is caused by two assumptions adopted in the theory. First, the microgel elliptical shape is not justified for loosely cross-linked microgels, especially at high χ_{AB} . The shape deviation is seen in Fig. 6 at $a_{AB} = 60$ and has been discussed in ref. 18 in detail. The second assumption concerns constancy of the polymer volume fraction within the microgel. In fact, for highly incompatible liquids, the microgel density reaches a maximum value exactly at the phase boundary to diminish the number of unfavourable A–B contacts (see Fig. 13c and discussion below or ref. 23). Thus, contraction of the whole microgel is not required to lower an excess interfacial energy since the latter can be achieved by

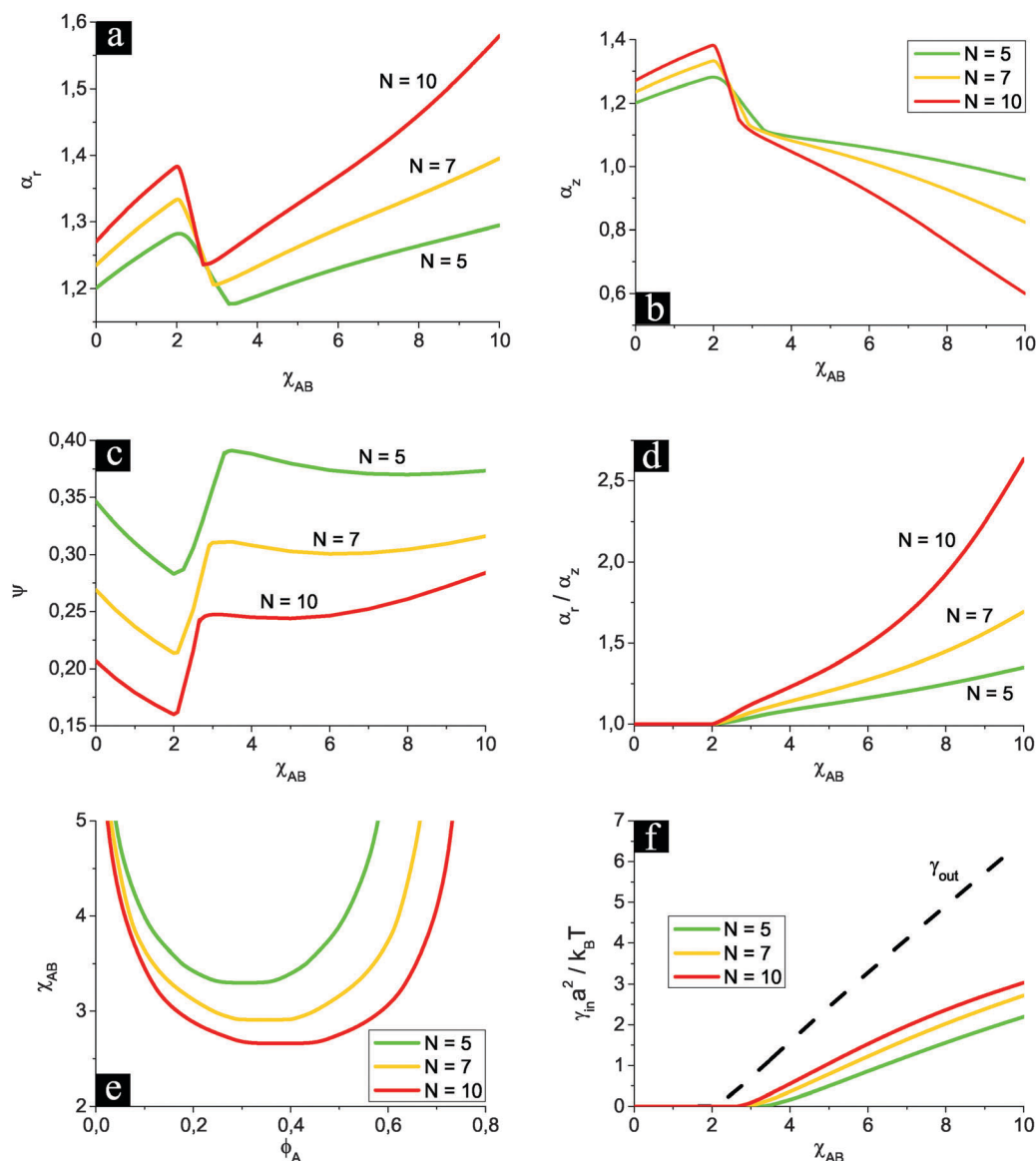


Fig. 9 Theory. Lateral (a) and normal (b) microgel swelling ratios, polymer volume fraction within the microgel (c), microgel aspect ratio α_r/α_z (d), interfacial tensions (f) vs. χ_{AB} and binodals of the mixture within the microgel (e) at $\chi_{AP} = 0$. The curves correspond to microgels of different subchain lengths: $N = 5$ and $\psi_0 = 0.6$ (green), $N = 7$ and $\psi_0 = 0.507$ (yellow), and $N = 10$ and $\psi_0 = 0.424$ (red).

redistribution of polymer density toward the internal phase boundary.

C Effect of the solvent quality. The above theoretical calculations deal with the case of a good solvent, $\chi_{AP} = 0$. As the solvent quality worsens, microgel swelling goes down and the range of miscibility of the liquids inside the particle broadens. Comparison of the binodals in θ -solvent ($\chi_{AP} = 0.5$) and good solvents ($\chi_{AP} = 0.25$ and $\chi_{AP} = 0$) is done in Fig. 11. We can see that the miscibility of the liquids inside the microgel is better for the θ -solvent. If χ_{AP} exceeds 0.5, both liquids become poor solvents for the microgel. To describe such a case, it is necessary to modify the developed theory by addition of a term responsible for the excess free energy at the external surface of a collapsed microgel.¹⁹ However, qualitative predictions on the behavior of the system in the poor solvents can be done without rigorous calculations: a

further increase of χ_{AP} above 0.5 should enhance the miscibility of the liquids. Similarly to the increasing cross-link density, decreasing solvent quality leads to a higher microgel surface activity, *i.e.* higher values of $(\gamma_{out} - \gamma_{in})$. These results coincide with experimentally observed diminution of oil–water interfacial tension at increasing temperature provoking collapse of microgels adsorbed at this interface.¹⁰

The case of the microgel placed at the interface of two equally poor solvents was studied using the DPD computer simulations. The values of R_r and R_z vs. χ_{AB} are plotted in Fig. 12 for the liquids both being good or poor solvents. First, in the range $0 < \chi_{AB} < 2$ the microgel swelling is isotropic, and the components of the gyration radius satisfy condition $R_r = \sqrt{2}R_z$ valid for the sphere. Above $\chi_{AB} = 2$, the microgel undergoes flattening in both poor and good solvents. Interestingly, the

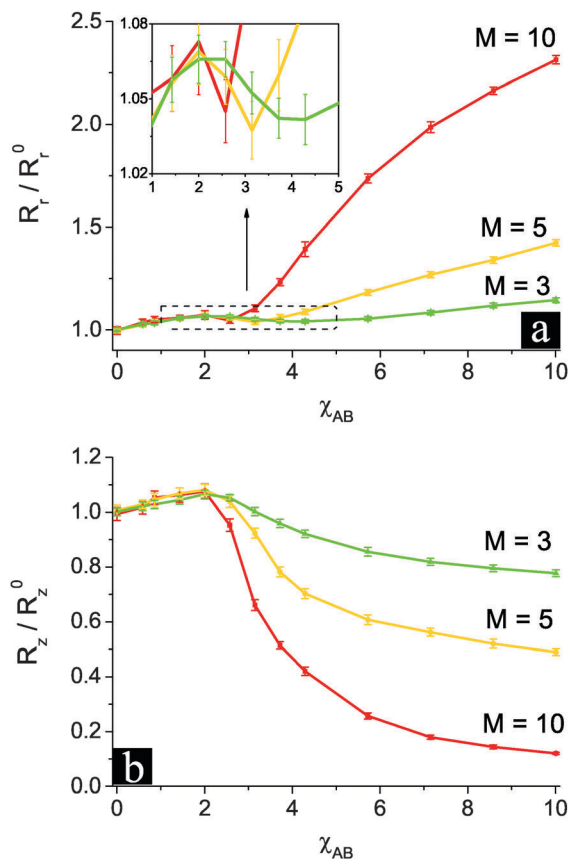


Fig. 10 Computer simulations. Lateral, R_t/R_t^0 , and normal, R_z/R_z^0 , components of the gyration radius of the adsorbed microgel as a function of the interaction parameter χ_{AB} at $\chi_{AP} = \chi_{BP} = 0$ ($a_{AP} = a_{BP} = 25$). The curves correspond to the microgels differing in the number of beads in the subchain, $M = 3, 5$ and 10 , and having approximately equal total numbers of beads: 8039, 8025 and 8049, respectively. The inset corresponds to a zoom in the range $1 < \chi_{AB} < 5$, where the graphs change in a non-monotonous way.

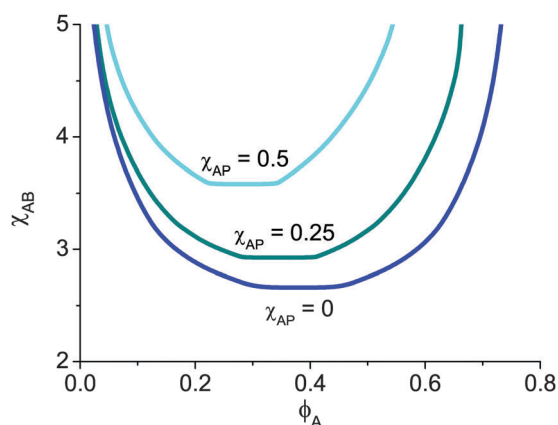


Fig. 11 Theoretical binodals of phase separation of the liquids within the microgel for different solvent qualities: $\chi_{AP} = 0, 0.25$ and 0.5 . $\psi_0 = 0.6$, and $N = 10$ and $\nu = 5 \times 10^3$.

microgel lateral dimensions in the poor solvent do not reveal non-monotonicity with increasing incompatibility of the liquids.

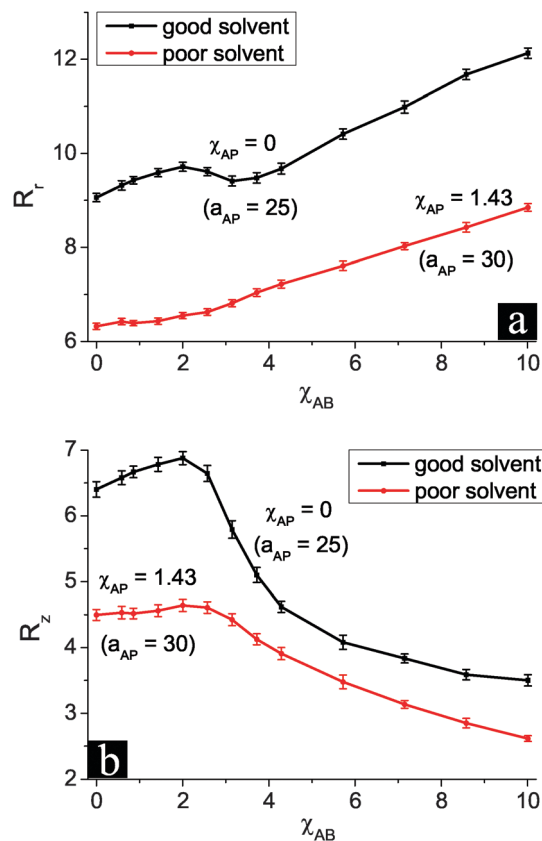


Fig. 12 Computer simulations. Effect of solvent quality on the lateral, R_t , and normal, R_z , microgel dimensions. Black and red curves correspond to the good ($a_{AP} = 25$, i.e. $\chi_{AP} = 0$) and poor ($a_{AP} = 30$, i.e. $\chi_{AP} = 1.43$) solvents, respectively. Each subchain contains $M = 5$ beads; the total number of beads in the microgel is 12 066.

Fig. 13 shows the density profiles (volume fractions) of both A and B liquids and the polymer along the normal Z-axis. To calculate them within the microgel, the averaging over the microgel central part limited by one third of its Z-axis gyration radius was performed. In the central part of the microgel its Z-thickness hardly depends on the lateral coordinates, see **Fig. 6**. The total microgel Z-thickness decreases with increasing χ_{AB} for both good and poor solvents (**Fig. 13a** and **c**).

The polymer volume fraction within the microgel depends on the solvent quality of A and B liquids. In the case of good solvent, $\chi_{AP} = 0$ (**Fig. 13a** and **c**), it changes as the incompatibility of the liquids increases; the average value is around $\psi \approx 0.3$. At $\chi_{AB} = 2.57$ (**Fig. 13a**), slightly above the point of the phase separation in the outer solution $\chi_{AB} = 2$, it occurs to be somewhat lower, $\psi = 0.28$, and for highly incompatible liquids, $\chi_{AB} = 7.14$, it is slightly higher, $\psi = 0.33$. One can roughly estimate $\chi_{AB}^{\text{bin}} \approx 3$ and find that the theory accords with the simulations: the liquids are mixed below this threshold (**Fig. 13a**) while two (micro)phases are formed within the microgel above this value (**Fig. 13c**). The peak of the polymer density in the vicinity of $Z = 0$ provides diminution of the number of unfavourable contacts between A and B molecules at the interface of (micro)phases.²³

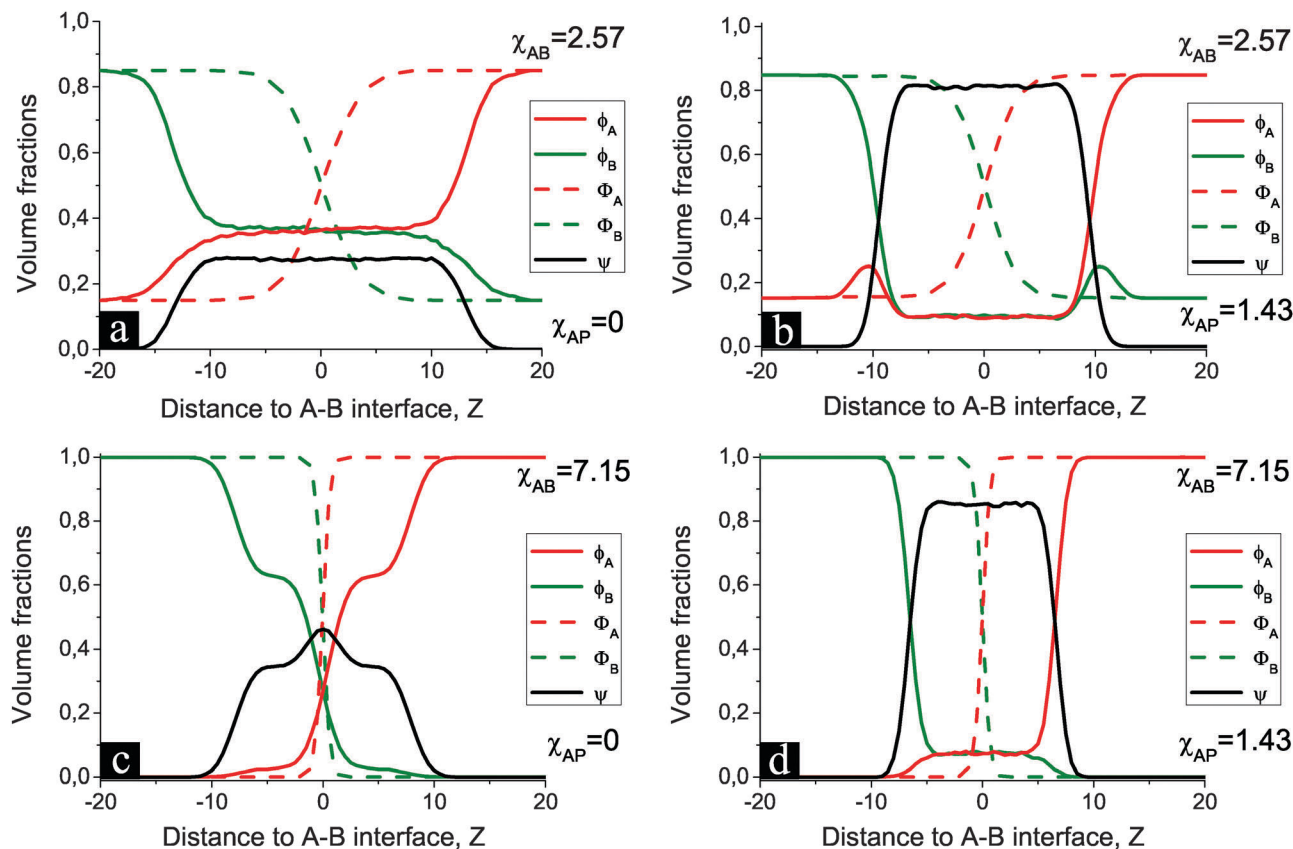


Fig. 13 Computer simulations. Volume fractions of A and B liquids, and polymers as a function of normal coordinate Z (red, green and black curves, respectively). Solid lines (ϕ_A , ϕ_B and ψ) correspond to the profiles passing through the microgel. Dashed lines (Φ_A and Φ_B) are those outside the microgel. Top and bottom rows correspond to moderately ($a_{AB} = 34$, *i.e.* $\chi_{AB} = 2.57$) and highly ($a_{AB} = 50$, *i.e.* $\chi_{AB} = 7.14$) immiscible liquids, respectively. Left and right columns depict cases when the liquids are good ($a_{AP} = 25$, *i.e.* $\chi_{AP} = 0$) and poor ($a_{AP} = 30$, *i.e.* $\chi_{AP} = 1.43$) solvents for the microgel, respectively. Each subchain consists of $M = 5$ beads; the total number of beads in the microgel is 12 066.

The microgel density at the interface of two poor solvents, $\chi_{AP} = 1.43$ (Fig. 13b and d), remains almost unchanged, $\psi = 0.83$, at any degree of immiscibility of the liquids. The threshold value of the FH interaction parameter provoking (micro)phase separation appears to be very high, $\chi_{AB}^{\text{bin}} \approx 12$, so that the liquids form a homogeneous mixture in the whole studied range of $\chi_{AB} \leq 10$, *e.g.* at $\chi_{AB} = 7.14$ (Fig. 13d).

The local maxima in concentrations of the A and B liquids appear near the microgel surfaces at $\chi_{AB} = 2.75$ and $\chi_{AP} = 1.43$ (Fig. 13b). They resemble a non-selective solvent concentrating at the interface of polymer domains in microphase separated block-copolymers^{46,47} to reduce the interfacial tension.

5 Conclusions

In the present theoretical and computer simulation studies, swelling and collapse of a single polymer microgel at the interface of two immiscible liquids have been examined by means of the Flory–Huggins lattice model and dissipative particle dynamics. The symmetric case, when molecules of both liquids interact with the polymer equally, was studied.

If the liquids are highly immiscible, the microgel interior segregates into two (micro)phases of equal volumes, both with equal polymer content but each enriched with the corresponding liquid. In the case of relatively moderate immiscibility, a homogeneous mixture of liquids inside the whole microgel is the thermodynamically favorable state of the system. The enhanced miscibility of the liquids inside the microgel as compared to the outer solution is due to the decrease of the number of unfavorable interactions between their molecules, while the entropy of mixing remains unchanged, $k_B \ln 2$ per molecule. Binodals of the mixture of the liquids within the microgel are plotted and interfacial tension values within and out of it are calculated. At any degree of immiscibility of the liquids, the presence of the microgel at the interface leads to the decrease of the interfacial tension, which in turn causes microgel flattening restrained by elasticity of stretched polymer subchains. The microgel at the interface undergoes anisotropic deformation: it is elongated in the lateral directions and flattened in the normal one. Low cross-link density and small dimensions facilitate the microgels to adopt a flattened shape. Higher reduction of interfacial tension is exhibited by densely cross-linked particles.

Acknowledgements

The financial support of the Russian Science Foundation, project 15-13-00124, the Deutsche Forschungsgemeinschaft within SFB 985 and the Volkswagen Foundation is gratefully acknowledged. The simulations were performed on multiteraflop supercomputer Lomonosov at Moscow State University.

References

- J. I. Amalvy, S. P. Armes, B. P. Binks, J. A. Rodrigues and G.-F. Unali, *Chem. Commun.*, 2012, **14**, 1826–1827.
- S. Fujii, E. S. Read, B. P. Binks and S. P. Armes, *Adv. Mater.*, 2005, **17**, 1014–1018.
- T. Ngai, S. H. Behrens and H. Auweter, *Chem. Commun.*, 2005, 331–333.
- W. Richtering, *Langmuir*, 2012, **28**, 17218–17229.
- V. Schmitt and V. Ravaine, *Curr. Opin. Colloid Interface Sci.*, 2013, **18**, 532–541.
- W. Ramsden, *Proc. R. Soc.*, 1903, **72**, 447–486.
- S. U. Pickering, *J. Chem. Soc.*, 1907, **91**, 2001–2021.
- B. Brugger, B. A. Rosen and W. Richtering, *Langmuir*, 2008, **24**, 12202–12208.
- M. Destribats, V. Lapeyre, E. Sellier, F. Leal-Calderon, V. Schmitt and V. Ravaine, *Langmuir*, 2011, **27**, 14096–14107.
- Y. Wu, S. Wiese, A. Balaceanu, W. Richtering and A. Pich, *Langmuir*, 2014, **30**, 7660–7669.
- M. Destribats, V. Lapeyre, M. Wolfs, E. Sellier, F. Leal-Calderon, V. Ravaine and V. Schmitt, *Soft Matter*, 2011, **7**, 7689–7698.
- T. Schmidt, S. Liu, S. Rutten, K.-H. Phan, M. Moeller and W. Richtering, *Langmuir*, 2011, **27**, 9801–9806.
- K. Geisel, L. Isa and W. Richtering, *Langmuir*, 2012, **28**, 15770–15776.
- K. Geisel, K. Henzler, P. Guttmann and W. Richtering, *Langmuir*, 2015, **31**, 83–89.
- S. Wiese, A. C. Spiess and W. Richtering, *Angew. Chem., Int. Ed.*, 2013, **52**, 576–579.
- H. Monteillet, M. Workamp, J. Appel, J. M. Kleijn, F. A. M. Leermakers and J. Sprakel, *Adv. Mater. Interfaces*, 2014, **1**, 1300121.
- D. M. Kaz, R. McGorty, M. Mani, M. P. Brenner and V. N. Manoharan, *Nat. Mater.*, 2012, **11**, 138–142.
- A. Mourran, Y. Wu, R. A. Gumerov, A. A. Rudov, I. I. Potemkin, A. Pich and M. Moeller, *Langmuir*, 2016, **32**, 723–730.
- J.-M. Y. Carrillo, E. Raphael and A. V. Dobrynin, *Langmuir*, 2010, **26**, 12973–12979.
- T. Salez, M. Benzaquen and E. Raphael, *Soft Matter*, 2013, **9**, 10699–10704.
- Z. Cao and A. V. Dobrynin, *Macromolecules*, 2015, **48**, 443–451.
- L. Isa, E. Amstad, K. Schwenke, E. Del Gado, P. Ilg, M. Kroeger and E. Reimhult, *Soft Matter*, 2011, **7**, 7663–7675.
- R. A. Gumerov, A. M. Rumyantsev, A. A. Rudov, A. Pich, W. Richtering, M. Moeller and I. I. Potemkin, *ACS Macro Lett.*, 2016, **5**, 612–616.
- P. K. Jha, F. J. Solis, J. J. de Pablo and M. Olvera de la Cruz, *Macromolecules*, 2009, **42**, 6284–6289.
- P. K. Jha, J. W. Zwanikken and M. Olvera de la Cruz, *Soft Matter*, 2012, **8**, 9519–9522.
- P. J. de Gennes, *Scaling Concepts in Polymer Physics*, Cornell University, Ithaca, 1979.
- A. Y. Grosberg and A. R. Khokhlov, *Polymer Physics*, AIP Press, New York, 1994.
- P. J. Flory, *Principles of Polymer Chemistry*, Cornell University Press, Ithaca, NY, 1953.
- J. A. Barker and W. Fock, *Discuss. Faraday Soc.*, 1953, **15**, 188–195.
- J. G. Jung and Y. C. J. Bae, *Polym. Sci., Ser. B*, 2010, **48**, 162–167.
- J. S. Choi, H. E. Yang, C. H. Lee and Y. C. Bae, *Fluid Phase Equilib.*, 2014, **380**, 100–115.
- Y. Hu, S. M. Lambert, D. S. Soane and J. M. Prausnitz, *Macromolecules*, 1991, **24**, 4356–4363.
- M. Quesada-Perez, J. A. Maroto-Centeno, J. Forcada and R. Hidalgo-Alvarez, *Soft Matter*, 2011, **7**, 10536–10547.
- J. W. Cahn and J. E. Hilliard, *J. Chem. Phys.*, 1958, **28**, 258–267.
- A. M. Rumyantsev, A. A. Rudov and I. Potemkin, *J. Chem. Phys.*, 2015, **142**, 171105.
- R. Schroeder, A. A. Rudov, L. A. Lyon, W. Richtering, A. Pich and I. I. Potemkin, *Macromolecules*, 2015, **48**, 5914–5927.
- K. Geisel, A. Rudov, I. I. Potemkin and W. Richtering, *Langmuir*, 2015, **31**, 13145–13154.
- R. Groot and P. Warren, *J. Chem. Phys.*, 1997, **107**, 4423–4435.
- A. Maiti and S. J. McGrother, *J. Chem. Phys.*, 2004, **120**, 1594–1601.
- Y. E. Kirsch, *Prog. Polym. Sci.*, 1993, **18**, 519–537.
- S. G. Starodubtzev, V. R. Ryabina, V. V. Vasilevskaya and A. R. Khokhlov, *Polym. Sci., Ser. A*, 1989, **31**, 713–718.
- P. G. de Gennes, *J. Phys. Lett.*, 1976, **37**, 59.
- K. Binder, *Adv. Polym. Sci.*, 1994, **112**, 181–299.
- M. Rubinstein and R. H. Colby, *Polymer Physics*, Oxford University Press, Oxford, UK, 2003.
- P. Kosovan, T. Richter and C. Holm, *Macromolecules*, 2015, **48**, 7698–7708.
- A. A. Rudov, E. S. Patyukova, I. V. Neratova, P. G. Khalatur, D. Posselt, C. M. Papadakis and I. I. Potemkin, *Macromolecules*, 2013, **46**, 5786–5796.
- A. Stenbock-Fermor, A. A. Rudov, R. A. Gumerov, L. A. Tsarkova, A. Boeker, M. Moeller and I. I. Potemkin, *ACS Macro Lett.*, 2014, **3**, 803–807.